ANL/TD/CP-96465





# Laser Beam Welding of AZ31B-H24 Magnesium Alloy

K.H. Leong, G. Kornecki, P.G. Sanders, and J.S. Keske

Technology Development Division
Argonne National Laboratory
9700 S. Cass Avenue, Building 207
Argonne, IL 60439

## ABSTRACT

The laser beam weldability of AZ31B magnesium alloy was examined with high power CW $CO_2$ and pulsed Nd:YAG lasers. The low viscosity and surface tension of the melt pool make magnesium more difficult to weld than steel. Welding parameters necessary to obtain good welds were determined for both CW $CO_2$ and pulsed Nd:YAG lasers. The weldability of the magnesium alloy was significantly better with the Nd:YAG laser. The cause of this improvement was attributed to the higher absorption of the Nd:YAG beam. A lower threshold beam irradiance was required for welding, and a more stable weldpool was obtained.

## INTRODUCTION

Cast and wrought magnesium alloys have the potential to replace steel and aluminum alloys in many structural or mechanical applications. They are strong, light-weight structural materials with strengths comparable to strong aluminum alloys. With densities 36% less than aluminum and 78% less than steel, magnesium alloys have excellent strength to weight ratios. Because of their hexagonal close-packed (HCP) crystal structure, they exhibit limited ductility at room temperature, but are easily extruded at elevated temperatures. Magnesium alloys also have excellent sound damping capabilities [1].

Current magnesium alloy applications are in areas with a specific need for lightweight components such as in some indusrial machinery and in aerospace equipment. The primary barrier to the increased use of magnesium alloys is cost. Although the metal is widely available in seawater (0.13%), magnesium costs up to 6 times as much as steel and as much as twice that of aluminum on a mass basis [2]. The price differential is considerably less on a volume basis. The true production cost of magnesium could be substantially reduced by increased demand driven by process research and development.

AZ31B is an all-purpose wrought alloy with good strength and ductility. It has excellent arc weldability but the process is slow and requires a filler material and post-weld heat treatments [1]. Surface preparation is crucial to obtaining sound welds. Arc welding of magnesium is too slow for optimal mass production of automotive components. If sound welds can be produced using laser beam welding, the above disadvantage could be overcome.

Laser beam welding has not been widely applied to magnesium alloys. Baeslack et al. laser welded a high strength magnesium casting alloy (5 wt% Y, 2 wt% Nd) and had problems with heat affected zone liquation cracking [3]. Chen et al. were able to obtain deep penetration welds in cast magnesium (4.5 mm at 1 kW) with relatively low laser power [4]. Recently, Niemeyer et al. have laser welded magnesium alloys (including AZ31B) with Nd:YAG and $CO_2$ lasers [5]. They were able to produce sound welds with minimal undercut using a CW Nd:YAG laser. The autogenous welds exhibited little change in hardness but had only about one third the tensile ductility at room temperature. Deep drawing the laser welded sheets was still possible at elevated temperatures.

## DISCLAIMER

This study examines the conditions for laser beam welding of AZ31B-H24 magnesium alloys in more detail. Welds were carried out with Nd:YAG and $CO_2$ lasers. Absorptivity effects on threshold irradiances and weldability of butt joints were examined. Weld hardness profiles were determined and compared with the microstructure of the weld and heat affected zone. Chemical analyses of the weld were carried out to determine loss of alloying elements and oxidation. The results augment the magnesium laser welding work of Niemeyer et al [5].

## EXPERIMENTAL CONDITIONS

Laser beam welding (bead-on-plate and butt) was performed on samples of 1.8 mm (nominal thickness) magnesium alloy AZ31B-H24 which has a nominal composition of 3 wt% Al and 1 wt% Zn. The H24 condition refers to strain hardening and partial annealing (recrystallization with no grain growth). The alloy sheets was supplied with a protective chromate conversion coating. Surfaces and edges were cleaned with acetone before welding. Chemical analysis for Al, Zn, and O was carried out by Wah Chang Analytical (Albany, Oregon). The metallic elements were measured by direct current plasma (DCP) spectroscopy, while the oxygen was quantified with a standard Leco test. A comparison of the ASTM alloy specifications for AZ31B-H24 [6] and the measured composition is given in Table 1.

**Table 1. Composition of Magnesium Alloy AZ31B (wt%)**

| | Al | Zn | Mn | Si | Cu | Ca | Ni | Fe | Mg | O (ppm) |
|---|---|---|---|---|---|---|---|---|---|---|
| Specification | 2.5 - 3.5 | 0.7 - 1.3 | 0.2 min | 0.05 max | 0.05 max | 0.04 max | 0.005 max | 0.005 max | balance | none |
| Measured | 3.27 | 0.79 | - | - | - | - | - | - | balance | < 50 |

A 2.0 kW pulsed Nd:YAG laser (Electrox) with fiberoptic beam delivery was used. The fiber size was 1 mm and 50 mm diameter lenses were used in the output optics. A 75 mm focal length lens focused the upcollimated beam from the fiber to a spot of 600 μm. Top gas shielding was provided by a 40 lpm flow of argon in a trailing jet configuration delivered by a 0.8 cm diameter tube oriented at 45° from the surface and 1 cm from the weld. Bottom shielding was accomplished with a 20 lpm flow of argon within a rectangular slot below the butt joint seam. The optics were protected by an air knife with a 50 lpm flow of nitrogen.

Welds were also obtained with a 6 kW CW $CO_2$ laser (Rofin Sinar RS6000) using a near $TEM_{20}$ ($M^2$=4.1) beam and a 150 mm focal length off-axis parabola. The spot size of the focused beam was 400 μm. Top gas shielding was provided by a flow of helium in a trailing or transverse jet configuration delivered by a 0.5 cm diameter tube oriented at 45° from the surface and 1 cm from the weld or by a special shroud that ensures oxygen free shielding of the weld area [7]. Bottom shielding was accomplished with a 25 lpm flow of helium within a rectangular slot below the butt joint seam. The optics were protected by a crossflow device (Spawr Industries) with a 100 lpm flow of nitrogen.

The weld, heat affected zone, and the base material were examined by optical microscopy. Transverse cross-sections of the autogenous welds were metallographically prepared and etched with dilute Keller's reagent to determine penetration depth and weld microstructure. Vickers microhardness measurements were made every 0.2 mm across the weld using a 50 g load and a dwell time of 15 s.

## RESULTS AND DISCUSSION

### Welding Parameters

The thermophysical properties of magnesium, alloying elements and iron are listed in Table 2 [8-11]. The properties affect the beam irradiance required for welding and the overall weldability of the alloy [11, 12]. The viscosity and surface tension of molten magnesium at the melting point are lower than those of aluminum and substantially lower than those of steel. These low values contribute to an unstable weldpool, production of substantial spatter and poor weld surface quality [12]. At weldpool temperatures, the relatively high vapor pressures of magnesium and zinc, as compared to

aluminum, indicate that only magnesium and zinc will have significant evaporative losses during welding. Minimizing the irradiance incident upon the workpiece would reduce the spatter as well as loss of zinc. Therefore, the approach was to determine the threshold irradiance at which consistent coupling of the beam to the workpiece occurred so that the irradiance for achieving a prescribed penetration can be minimized. The welding speed was adjusted to provide the necessary penetration.

**Table 2. Thermophysical Properties of Al, Zn, Mg, and Fe.**

| | Al | Fe | Mg | Zn |
|---|---|---|---|---|
| Melting point $T_m$ (K) | 933 | 1808 | 923 | 693 |
| Boiling point $T_b$ (K) | 2333 | 3003 | 1380 | 1203 |
| Vapor pressure (Pa) @ $T_m$ | $10^{-6}$ | 2.3 | 360 | 23 |
| 1000K | 0.000012 | 0 | 1360 | 12000 |
| Viscosity (mPa s @ $T_m$) | 1.3 | 6 | 1.25 | 3.5 |
| Surface tension (N/m @ $T_m$) | 0.91 | 1.87 | 0.56 | 0.78 |
| Thermal conductivity of solid @ $T_m$ (W $m^{-1}K^{-1}$) | 210 | 30 | 130 | 9 |
| Absorptivity (%) @ $T_m$ 1.06 μm | 11 | 36(300K) | | 42(300K) |
| 10.6 μm | 3 | 5(300K) | 3(300K) | 10 |

Bead-on-plate (BOP) welds were used to develop the parameters for Nd:YAG laser welding of magnesium. Initially, the energy per unit time (peak irradiance) was reduced to a level which just produced consistent coupling (1.35 J/ms). Higher energy densities led to greater evaporation losses, increased spatter, and uneven weld beads. The pulse length was then increased until consistent weld bead appearance was obtained (5 ms). The maximum repetition rate (120 Hz) was constrained by the maximum duty cycle (60%). Finally, the travel speed was adjusted to produce full penetration (3 cm/s). For a travel speed of 3 cm/s and a beam diameter of 600 μm, the pulse overlap was 42%. The average power at the workpiece was 0.8 kW (1.3 kW peak), which led to a mean peak irradiance of 0.5 MW/$cm^2$. The mean irradiance corresponds to the ratio of 86% of the power over the cross-sectional area (containing 86% of the power) that was determined using a laser beam analyzer (Prometec).

Butt welds were made using parameters obtained from successful, full penetration bead-on-plate welds. These conditions produced sound butt welds in magnesium sheet with shear cut edges (see latter discussion and Y1 in Table 3 and Fig. 3a). The large beam diameter of the Nd:YAG laser made the welding quality less sensitive to small gaps in the shear cut edges. The use of argon cover gas, which is slightly denser than air, allowed good shielding of the workpiece evident by the shiny weld surface.

A model based on conservation of energy for a moving heat source incident on a flat plate was used to predict the threshold irradiance to initiate melting for the CW $CO_2$ laser [11]. The primary source of uncertainty in the calculation is the surface absorptivity. For a flat polished surface, the reference value of the absorptivity for 10.6 μm radiation at room temperature is 3% [13]. The threshold irradiance for melting with a travel speed of 12.7 cm/s and a beam diameter of 400 μm was calculated to be 1.5 MW $cm^{-2}$. The absorptivity of the AZ31B alloy was expected to be significantly higher because of the chromate conversion coating, which would result in a lower threshold irradiance.

BOP welds were also used to determine the average power and travel speed for $CO_2$ laser welding of magnesium. The BOP welds were made at a travel speed of 12.7 cm $s^{-1}$. The power was varied from 0.5 to 2 kW to produce mean irradiances ranging from 0.4 to 1.6 MW $cm^{-2}$. Consistent coupling occurred at an irradiance of 0.5 MW $cm^{-2}$, which is one third the value predicted for melting and approximately the minimum value required to sustain a keyhole [10]. Since the predicted value is a lower bound value for welding, the chromate coating must have increased the absorptivity from 3% (or a slightly higher value at the melting point) to >9% to allow consistent coupling at 0.5 MW/$cm^2$. The experimental threshold irradiance for chromate coated magnesium is less than

0.25 the value required for welding aluminum [12]. Removal of the chromate coating by polishing the sample caused an increase in the threshold irradiance required. At a spot size of 420 μm and a traverse speed of 12.7 cm $s^{-1}$, the threshold irradiances for welding were 0.42 MW $cm^{-2}$ for the magnesium with the chromate coating, 0.61 MW $cm^{-2}$ with the coating scrubbed off and 0.69 MW $cm^{-2}$ with a polished, shiny surface.

After determining the conditions for BOP welding with the $CO_2$ laser, butt welds with shear cut edges were attempted under similar conditions. In contrast to the Nd:YAG welding, the parameters for sound bead on plate welds did not directly translate into sound butt welds with or without the chromate coating. A sound weld is defined here as a full penetration weld with no significant cracks or porosity and good weld surface quality. Regardless of the travel speed or beam power used, full penetration welds could not be obtained. Improved welds were obtained by defocussing the beam or using mill edges as discussed in the weld microstructure section. However, regardless of the edge condition, the $CO_2$ welds were very sensitive to the process parameters used. There was a tendency for incomplete fusion of the edges of the plates. Magnesium has a higher oxidation potential than aluminum and the presence of the oxide layer on the surfaces of the edges may deter the joining process. The high peak power of the Nd:YAG laser beam would tend to break up the oxide layers better than the $CO_2$ case.

**Weld Microstructure and Hardness**

Welding parameters used to produce successful BOP welds and butt welds on shear-cut and milled edges are listed in Table 3. The corresponding micrographs of the transverse weld sections are shown in Figs. 1a-1e. The weld samples were etched in dilute Keller's reagent. The cross section of Nd:YAG weld Y1 (Fig. 1a) shows an absence of cracks or pores. A slight fitup problem is indicated with the small mismatch in the shear cut edges producing a concave top weld surface and some undulation of the bottom surface.

**Table 3. Autogenous Butt Welding Parameters**

| | Laser Beam | | | | Weld | | |
|---|---|---|---|---|---|---|---|
| | Power (kW) | Diameter (cm) | Irradiance ($MW/cm^2$) | Edge Condition | Speed (cm/s) | Width (cm) | Hardness Vickers |
| Base | | | | | | | 70 |
| Y1 | 0.8 | 0.06 | 0.5* | shear cut | 3.0 | 0.14 | 68 |
| C1 | 2.0 | 0.04 | 1.56 | BOP | 12.7 | 0.11 | |
| C16 | 3.5 | 0.1 | 0.45 | shear cut | 12.7 | 0.13 | 67 |
| C43 | 1.6 | 0.1 | 0.2 | milled | 0.64 | 0.30 | 59 |
| C47 | 2.5 | 0.04 | 2.0 | milled | 12.7 | 0.12 | 62 |

*peak irradiance

The cross section for a CW $CO_2$ BOP weld is shown in Fig. 1b. No pores or cracks are present. Initial welds using the CW $CO_2$ laser beam on shear cut edges were unsuccessful. Several approaches were used in attempts to improve the $CO_2$ laser welds. Fitup of the joint may have a significant effect on weldability when the focused beam size is comparable to the gap between the edges. The beam was defocused from 0.4 mm to 1 mm to reduce the sensitivity to fit-up. Improved welds were produced with higher power but still were not consistently sound welds (C16, Fig. 1c). The micrograph shows a few small pores but the tendency for dropout has depressed the top weld surface approximately 0.2 mm. In addition, a crack propagating from the top weld surface into the weld is evident. No improvements could be obtained with the chromate coating removed. With milled edges where the excellent fitup is equivalent to BOP condition, higher quality welds were obtained with the BOP welding parameters used for welds C43 (Fig. 1d) and C47 (Fig. 1e). The presence of pores in welds C16 and C47 which have the highest welding speed may be caused by the fast solidification of the weldpool trapping the vapor within pores near the surface. The other welds with slower welding

speeds have no pores.

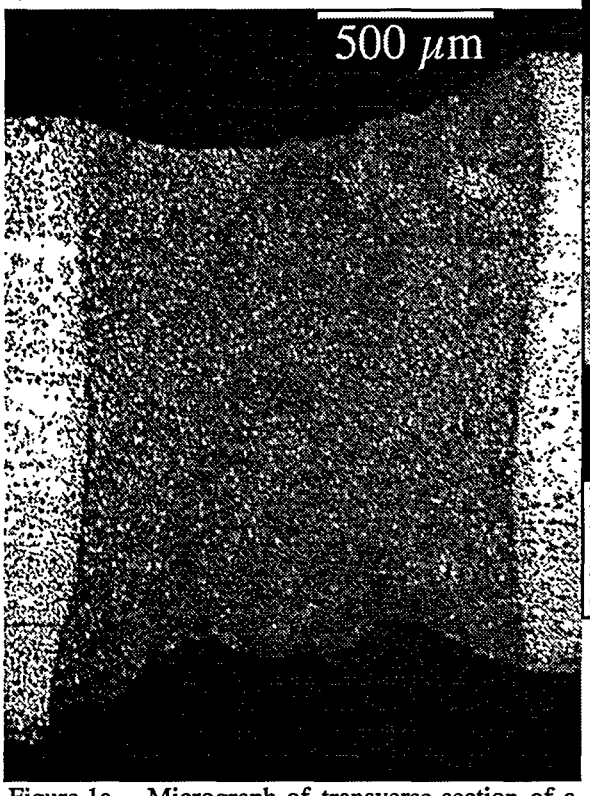


Figure 1a. Micrograph of transverse section of a pulsed Nd:YAG laser butt weld listed as Y1 in Table 3. Shear cut edges of the AZ31B sheet were used.

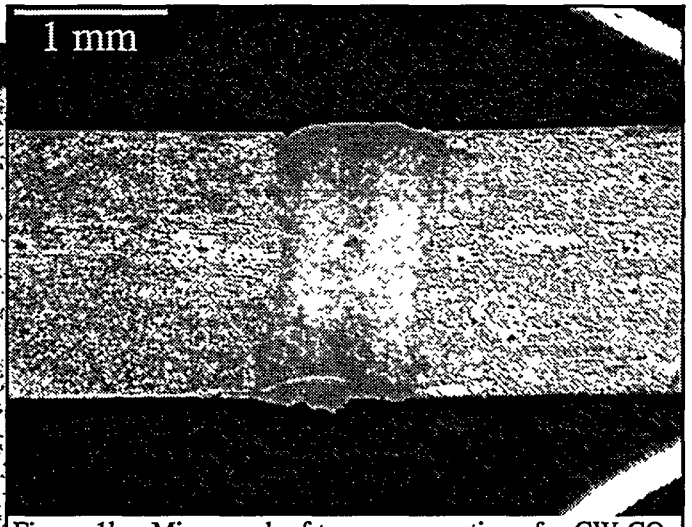


Figure 1b. Micrograph of transverse section of a CW $CO_2$ laser bead-on-plate weld listed as C1 in Table 3. The black spots on both the weld and base metal appear to be inclusions or artifacts of the polishing process.

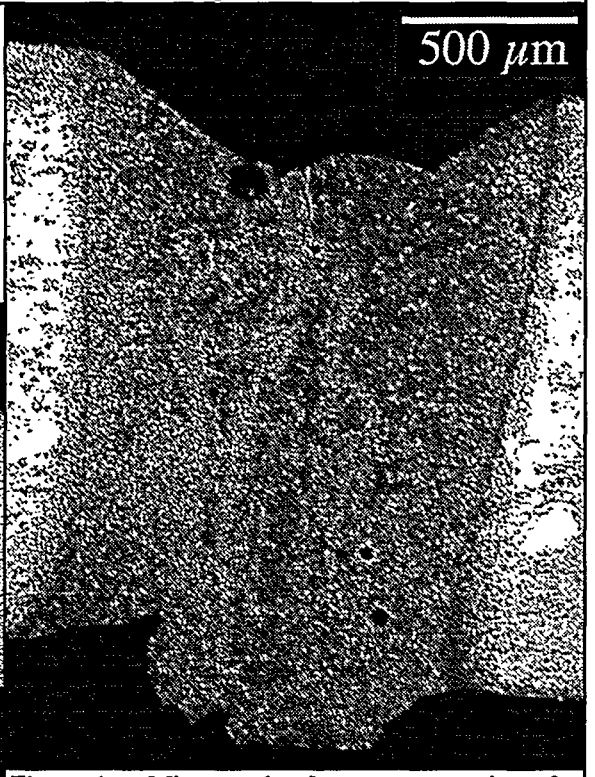


Figure 1c. Micrograph of transverse section of a CW $CO_2$ laser weld listed as C16 in Table 3. Shear cut edges of the AZ31B sheet were used. Pores and a crack from the middle of the top weld surface are evident.

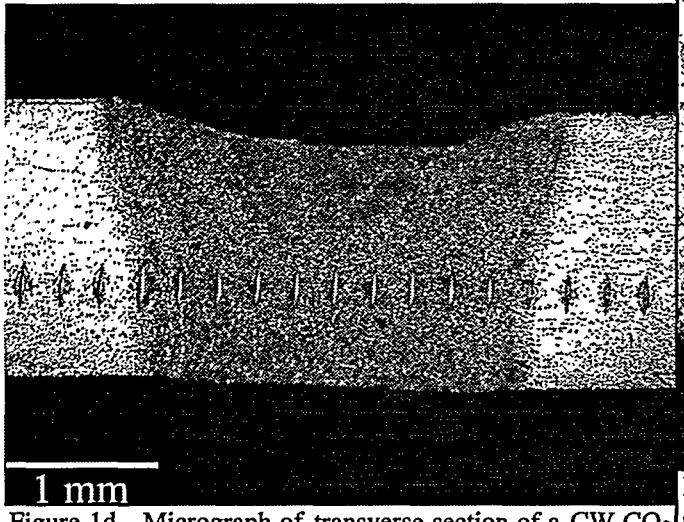


Figure 1d. Micrograph of transverse section of a CW $CO_2$ laser weld listed as C43 in Table 3. Milled edges of the AZ31B sheet were used. Knoop hardness indentations are visible. However, all reported hardness values are in Vickers.

The weld cross sections obtained were examined at higher magnification to examine effects of the welding parameters on weld microstructure. Similar the microstructural features in both the center a edge o fusion zone were found. The center of the weld bead had a dendritic single phase structure with relatively small grains as shown in Fig. 2, representative of a rapidly solidified material.

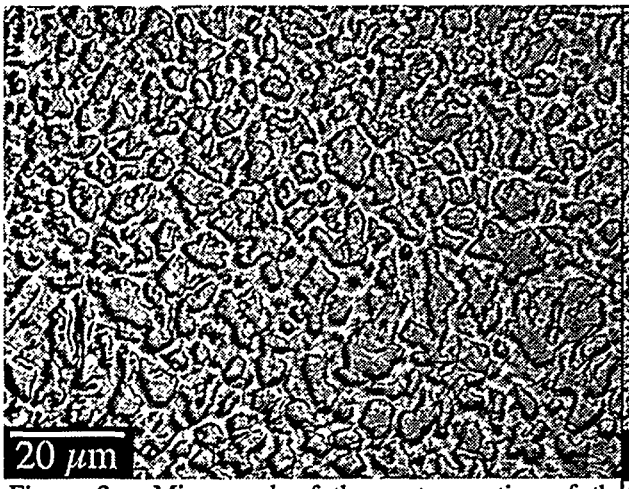


Figure 2. Micrograph of the center section of the Nd:YAG laser weld bead (weld Y1) showing microstructure.

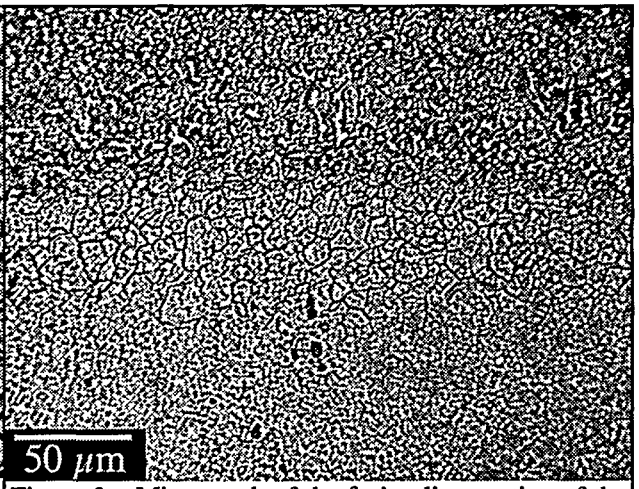


Figure 3. Micrograph of the fusion line section of the Nd:YAG laser weld bead (weld Y1) showing microstructure. The top of the figure is the weld metal side.

Fig. 3 shows a section from the weld metal to the base metal. The fusion line is evident from the change in microstructure between the weld metal and the heat affected zone. Near the fusion line, the dendrites were radially elongated toward the weld centerline. The width of the heat affected zone for welds Y1 and C47 were approximately 50 to 60 μm. The value for weld C43 with the substantially slower weld speed was approximately twice as wide. Rapid melting and resolidification during welding change the structure and properties of both the weld and the heat affected zone.

The microstructure of the weld is characteristic of a high speed process and develops when heat is rapidly extracted from the molten fusion zone by the surrounding base material. Heterogeneous nucleation occurs at the fusion line and dendrites would grow toward the heat source. Due to the high heat flux immediately around the fusion zone, coarsening of the initial microstructure can occur. This grain growth in the heat affected zone can be detrimental to the weld properties.

Very large grains in the heat affected zone are generally undesirable. With the increased heat during welding, alloying elements and impurities may segregate to the grain boundaries and embrittle this region. However, grain growth can be minimized with faster travel speeds. The grain size in the heat affected zones are much smaller at a travel speed of 12.7 cm/s (C47) than at 0.64 cm/s (C43) as shown in Fig. 4. Clearly, grain growth was much more prevalent in the weld made at the slower speed.

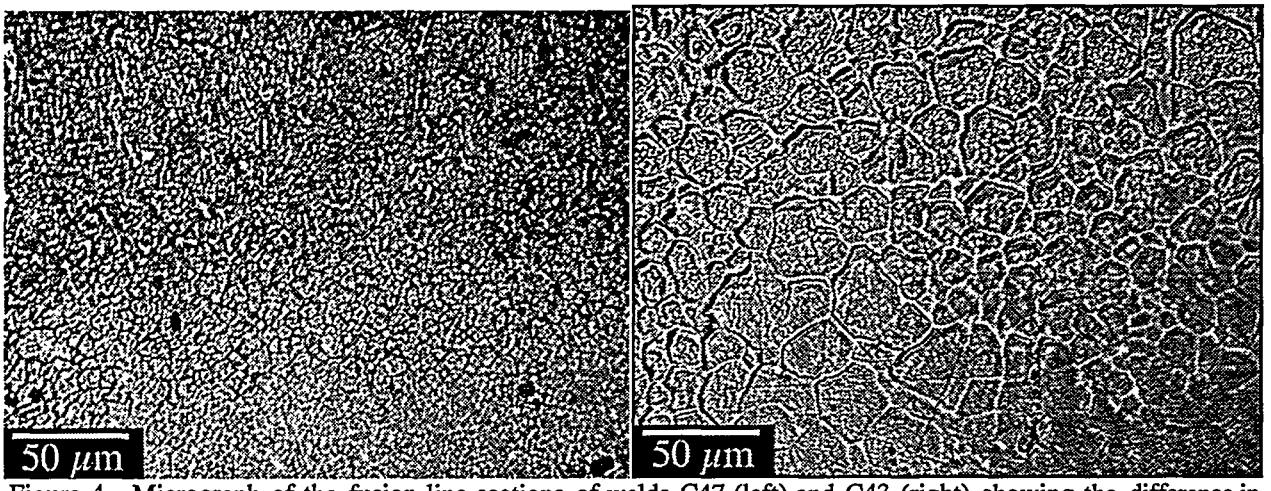


Figure 4. Micrograph of the fusion line sections of welds C47 (left) and C43 (right) showing the difference in microstructure when the weld speed is reduced from 12.7 cm $s^{-1}$ to 0.64 cm $s^{-1}$. The fusion line is approximately midway between the top and bottom of the micrographs.

The Vickers microhardness of each weld was determined from the average of 8 indentations across the weld (Table 3). The variation in the base metal hardness is due to inhomogeneities in the alloy. The profile obtained for weld C47 is shown in Fig. 5. Hardness profiles of the $CO_2$ welds showed a sequential decrease in the hardness from the base material through the heat affected zone to the fusion zone. The average hardness of the $CO_2$ welds decreased with decreased travel speed. The hardness of the heat affected zone was reduced as a result of grain growth (Figs. 3 and 4). Since this effect diminished with distance from the weld, the hardness increased with distance from the weld, eventually reaching the base material hardness. However, the Nd:YAG weld (Y1) did not have significant decrease in the hardness within the weld (Fig. 6). The base material in the H24 condition had an average Vickers microhardness of 70, while that of weld Y1 was 67. The heat affected zone was very narrow (< 0.1 mm), which helped maintain the base material hardness right up to the weld.

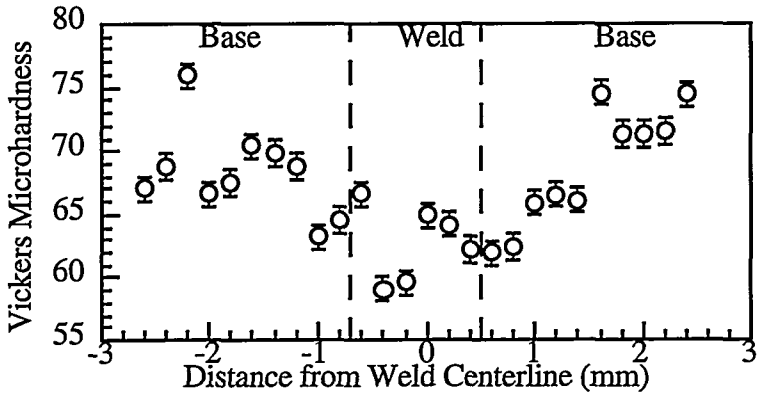


Figure 5. Microhardness profile of the weld zone, heat affected zone and base metal for weld C47 obtained using a $CO_2$ beam.

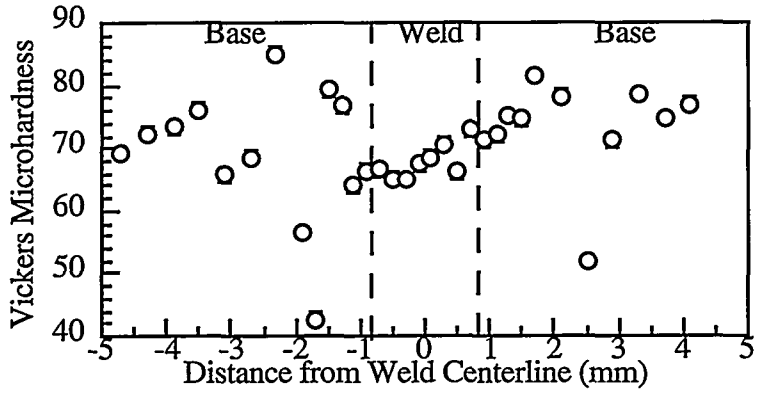


Figure 6. Microhardness profile of the weld zone, heat affected zone and base metal for weld Y1 obtained using a pulsed Nd:YAG beam.

**Weld Composition**

The weld beads of the four autogenous butt welds discussed above were analyzed for aluminum and zinc with DCP spectroscopy. A comparison of the aluminum and zinc concentrations in the base

material and the four weld beads is shown in the first two columns of Table 4. The concentrations of both aluminum and zinc increased, indicating a net magnesium loss. This is illustrated in the third column of Table 4, in which the magnesium fraction was calculated by assuming magnesium comprised the balance of the alloy.

**Table 4. Weld Bead Chemical Composition**

| | Al | Zn | Mg | No Al Loss (g/initial 100 g) | | | | % loss | | O (ppm) |
|---|---|---|---|---|---|---|---|---|---|---|
| | wt% | wt% | balance | Al | Zn | Mg | Total | Zn | Mg | |
| Base | 3.27 | 0.79 | 95.9 | 3.27 | 0.79 | 95.9 | 100 | | | < 50 |
| Y1 | 3.44 | 0.82 | 95.7 | 3.27 | 0.78 | 91.0 | 95 | 1.3 | 5.1 | < 50 |
| C16 | 3.45 | 0.81 | 95.7 | 3.27 | 0.77 | 90.7 | 95 | 2.5 | 5.4 | - |
| C43 | 3.84 | 0.86 | 95.3 | 3.27 | 0.73 | 81.2 | 85 | 7.6 | 15.3 | - |
| C47 | 3.76 | 0.87 | 95.4 | 3.27 | 0.75 | 82.9 | 87 | 5.1 | 13.6 | < 50 |

To understand compositional changes during welding in more detail, it is helpful to refer to some of the physical properties of Al, Zn, and Mg (Table 2). Both Zn and Mg have lower boiling points and higher vapor pressure than Al. The temperature of 1000K is representative of the weld temperature. At this temperature, the vaporization of aluminum is negligible compared to magnesium or zinc. Consequently, by assuming negligible aluminum loss, the weld composition can be computed as indicated in Table 4.

Laser welding studies of Al alloys containing Mg have found that Mg is the predominant component in the black coating deposited near the weld, even though Mg was a small fraction of the overall alloy [13]. Similar black coatings was obtained after welding the magnesium samples and would indicate the formation of ultrafine particles from the more volatile components of the alloy, i.e., Mg and Zn. As expected, the weld metal show losses of both Mg and Zn. It is interesting that the relative Mg loss is more than twice that for Zn even though the vapor pressure of pure Mg is substantially lower than that of Zn. Larger losses of both Mg and Zn were obtained with welds at slow travel speeds (C43) and high irradiances (C47). The 15% mass loss for weld C43 at low weld speeds is consistent with the high undercut evident in the cross section shown in Fig. 1d. Weld C47 also has a high mass loss (13%) but the weld cross section does not indicate so.

Laser welding of magnesium did not appear to increase the oxygen level in the weld above 50 ppm which was the detectabiltiy limit of the Leco technique. The oxygen level in the base material may be significantly lower than 50 ppm, so a small increase in oxygen with welding may occur without being detectable. Even low interstitial oxygen concentrations can be detrimental to the material properties. The data obtained indicate that the traditional gas shielding method was able to produce welds in magnesium with no measurable increase in the oxygen concentration.

## CONCLUSIONS

The above observations on weldability using a $CO_2$ beam are illustrative of the difficulties of using a high beam irradiance to weld a metal that has low viscosity and surface tension (in the molten state) and high oxidation potential. No such problems were encountered using the larger size Nd:YAG laser beam that coupled at a lower irradiance.

Welding parameters were determined for AZ31B-H24 magnesium sheet alloy for both pulsed Nd:YAG and CW $CO_2$ lasers. With the Nd:YAG laser and a travel speed of 3 cm/s, sound welds were produced with an average power of 0.8 kW (5 ms pulse width, 120 Hz) and shear cut edges. The peak power was 1.3 kW and the peak irradiance was 0.5 MW/cm$^2$. Sound welds were produced with the $CO_2$ laser at 12.7 cm/s and 2.5 kW, but only with milled edges. The smaller beam diameter of the $CO_2$ laser was very sensitive to poor fit-up. The protective chromate conversion coating on the magnesium increased the absorptivity of the alloy and allowed coupling at lower irradiances resulting in improved welds.

Chemical analysis of the weld beads revealed changes in the metallic composition but no increase in the oxygen content. Due to the low boiling points and high vapor pressures of magnesium and zinc, these elements were preferentially evaporated during welding. The Vickers hardness within the

weld was significantly lower than the base material, while the heat affected zone had an intermediate hardness. The heat affected zone is softer because of grain growth.

## ACKNOWLEDGEMENTS

This work was supported in part by the U.S. Department of Energy, Office of Energy Research Laboratory Technology Research Program and the Office of Advanced Automotive Technologies.

## REFERENCES

1. W. R. Oates, editor, *Welding Handbook*, Materials and Applications, pt. 1, vol. 3, 8th ed., American Welding Society, Miami, Florida, 121-162, 1996.

2. L. Gaines, R. Cuenca, F. Stodolsky and S. Wu, Analysis of the Potential for New Automotive Uses of Wrought Magnesium, Argonne National Laboratory, Center for Transportation Research, ANL-ESD-35, Argonne, IL, February 1996.

3. W. A. Baeslack, S. J. Savage, and F. H. Froes: *J. Mater. Sci. Let.*, 1986, vol. 5, pp. 935-9.

4. G. Chen, G. Roth, and F. Maisenhalder: *Laser und Optoelektronik*, 1993, vol. 25, pp. 43-7.

5. H. Haferkamp, F. Von Alvensleben, I. Burmester, and M. Niemeyer, : *Proc. ICALEO 97*, Laser Institute of America, Orlando, FL, 1997.

6. S Housh, B. Mikucki, and A. Stevenson, Properties of Magnesium Alloys in Metals Handbook, 10th Edition, Volume 2, "Properties and Selection: Nonferrous Alloys and Special-Purpose Materials", ASM International, Materials Park, OH.

7. Leong, K.H., K.R. Sabo, P.G. Sanders, and W.J. Spawr. "Laser Beam Welding of Aluminum Alloys." SPIE Proceedings, Lasers as Tools for Manufacturing II. Vol. 2993:(1997).

8. Toulokian, Y.S., Powell, R.W., Ho, C.Y. And Nicolaou, M.C. Thermal Conductivity Metallic Elements and Alloys, Thermophysical Properties of Matter, Vol. 1, New York: IFI/Plenum, 1970.

9. T. Iida and R. I. L. Guthrie The Physical Properties of Liquid Metals, Clarendon Press, Oxford, 1993.

10. Nonhof, C. J. "Material processing with Nd-lasers". Electrochemical Publications, Ayr, Scotland, 1988.

11. K. H. Leong, H. K. Geyer, K. R. Sabo, and P. G. Sanders: *J. Laser Appl.*,9, 227-232.

12. K. H. Leong, K. R. Sabo, P. G. Sanders, and W. J. Spawr (1997) Laser Beam Welding of Aluminum Alloys, SPIE Proceedings Vol. 2993 Lasers as Tools for Manufacturing II.

13. W. E. Forsythe: *Smithsonian Physical Tables*, 9th ed., Smithsonian Institution, Washington D.C., 1959.

14. J.-D. Kim, S. Katayama, M. Mizutani, and T. Takemoto: Rev. Laser Eng., 1996, vol. 24, pp. 996-1005.